

Distributed Transmit Beamforming: Design and Demonstration From the Lab to UAVs

Samer Hanna^{ID}, *Member, IEEE*, and Danijela Cabric, *Fellow, IEEE*

Abstract—Cooperating radios can extend their communication range by adjusting their signals to ensure coherent combining at a destination radio. This technique is called distributed transmit beamforming. Beamforming (BF) relies on the BF radios having frequency synchronized carriers and phases adjusted for coherent combining. Both requirements are typically met by exchanging preambles with the destination. However, since BF aims to increase the received power, the individually transmitted preambles are typically at low SNR and their lengths are constrained by the channel coherence time. These noisy preambles lead to errors in frequency and phase estimation, which result in randomly changing BF gains. To build reliable distributed BF systems, the impact of estimation errors on the BF gains need to be considered in the design. In this work, assuming a destination-led BF protocol and Kalman filter for frequency tracking, we optimize the number of BF radios and the preamble lengths to achieve reliable BF gain. To do that, we characterize the relations between the BF gains distribution, the channel coherence time, and design parameters like the SNR, preamble lengths, and the number of radios. The proposed relations are verified using simulations and via experiments using software-defined radios in a lab and on UAVs.

Index Terms—Distributed transmit beamforming, cooperative communications, UAVs.

I. INTRODUCTION

DISTRIBUTED transmit beamforming (BF) enables a group of radios to act as a virtual antenna array when cooperating to transmit a common message to a destination radio. By having N equal-power radios beamform, the received power at the destination can increase by up to N^2 ; N -fold due to transmit power increase and N -fold due to coherent combining [1]. The N^2 increase can theoretically provide up to N fold extension of communication range or, for the same received power, reduce the transmitted power from each radio by N [2]. Thus, BF can enable long-range communications from cooperating low power devices, unable to communicate individually with a remote destination or improve the energy efficiency by reducing the

energy transmitted from individual radios. This can be useful for applications like power-constrained internet of things devices (IoT) whether deployed indoors or outdoors [3] or remotely deployed UAVs [4] or ground robots performing search and rescue [5]. Depending on the specific deployment environment, the propagation environment and channel coherence time would vary, however, the cooperating radios are typically in proximity of each other and far from the destination.

For separate radios, having independent oscillators, to act as one virtual array, they need to synchronize their carrier frequencies and adjust the phases for coherent combining at the destination. Since signals combine over-the-air, both requirements need to be satisfied prior to transmitting the payload. The satisfaction of these requirements is typically performed by exchanging preambles with the destination for channel phase estimation and carrier frequency synchronization [2]. However, given that in a typical distributed BF scenarios the radios have low power and/or the destination is remote, the pre-BF SNR of individual radios is low, and there are errors in both channel estimation and destination-led frequency synchronization that cannot be neglected and would result in phase errors in the combining signals. These combining phase errors will lead to the BF gains being non-deterministic and less than N^2 . The BF gain degradation cannot always be mitigated, especially in high mobility radios like UAV-mounted, where the channel coherence time limits the preamble lengths and makes the combining phase errors inevitable. To build a reliable BF system despite of these errors, we need to specify the number of BF radios and the preamble lengths such that a minimum desired post-BF SNR is attained with a given probability.

Existing works have proposed many approaches for distributed BF leveraging different methods for over-the-air phase adjustment and frequency synchronization [3] as wired solutions are not suitable for independent radios [6]. Approaches for phase adjustment include explicit channel feedback from the destination [7], 1-bit feedback where the BF radios iteratively adjust their phase based on binary feedback from the destination [8], and roundtrip message exchange among the destination and BF radios [9]. Unlike the other approaches, explicit channel estimation is non-iterative making it less complicated and more reliable specially under fast varying channels like those experienced by UAVs. For frequency synchronization, some works have relied on external frequency references like GPS [10], [11], out of band signaling [12], and others relied on a destination preamble along with averaging

Manuscript received 26 October 2021; revised 8 February 2022, 16 May 2022, and 6 August 2022; accepted 8 August 2022. Date of publication 18 August 2022; date of current version 13 February 2023. This work was supported in part by NSF under Grant 1929874; and in part by the CONIX Research Center, one of six centers in JUMP, a Semiconductor Research Corporation (SRC) Program sponsored by DARPA. The associate editor coordinating the review of this article and approving it for publication was G. Geraci. (Corresponding author: Samer Hanna.)

The authors are with the Electrical and Computer Engineering Department, University of California, Los Angeles, CA 90095 USA (e-mail: samerhanna@ucla.edu; danijela@ee.ucla.edu).

Color versions of one or more figures in this article are available at <https://doi.org/10.1109/TWC.2022.3198102>.

Digital Object Identifier 10.1109/TWC.2022.3198102

1536-1276 © 2022 IEEE. Personal use is permitted, but republication/redistribution requires IEEE permission. See <https://www.ieee.org/publications/rights/index.html> for more information.

filters like the the extended Kalman filter (EKF) for tracking the carrier drift [13], [14]. Filtering based approaches do not require additional bandwidth and do not rely on GPS signals which can be unavailable to ground robots or UAVs deployed indoor [15]. Also filtering based approaches have the potential to provide higher accuracy synchronization than GPS methods [16], [17]. While these works have proposed interesting approaches, the relation between the BF gains and the pre-BF SNR, necessary for designing a reliable BF system, was not analyzed. In [18], the sources of phase noise in reference oscillator were analyzed along with their impact on the distributed beamforming performance, however, the impact of the SNR of the exchanged preambles was not discussed.

Using the aforementioned approaches, several distributed BF demonstrations were carried out; in controlled lab experiments, 1-bit feedback was demonstrated using EKF for frequency synchronization in [13], [14], and [19] and out-of-band signaling in [12]. In [14], the BF procedure was designed for wireless power transfer compatible with 802.11 standard. Outdoor ground based demonstrations spanning several kilometers using explicit channel feedback were performed in [10] and [11] relying on GPS for frequency synchronization. Using explicit feedback, in [17], BF was demonstrated from UAVs with the synchronization performed over wires attached to the flying UAVs. These works have shown the potentials for distributed BF in signal combining, yet their results are hard to generalize to different scenarios because they are mostly empirical.

Other works have considered different distributed BF approaches to avoid signal exchange with the destination. In [20] and [21], distributed BF using radio locations was proposed assuming the knowledge of the direction towards the destination radio. However, these approaches are sensitive to localization errors and require sub-wavelength level localization accuracy [22], which might not be available and, additionally, the direction of the destination might be unknown for instance when a UAV is collecting measurements from BF IoT devices [23]. Another approach avoids destination feedback by repeating transmissions relying on the randomness of the combining gains [24]. However, this approach has a low throughput. BF using destination feedback does not require repeated transmissions and would work in a non-LOS channel without requiring any location information. Other works have also considered optimizing the BF radio locations [25], [26], however, in many cases the BF radios locations are predetermined and cannot be changed.

In this paper, we consider a destination-led BF protocol using the Kalman filter (KF) for frequency synchronization and explicit channel feedback. For that protocol, assuming equal pre-BF SNRs, we propose an analytical framework relating the statistical distribution of the BF gains, with the system parameters including pre-BF SNR, the number of BF radios, and the BF overheads (the duration of the exchanged preambles). Using this framework, we can optimize some of the system parameters to design a distributed BF system attaining a minimum required SNR with a given probability. To derive this framework, we derive the variance of the combining phase errors, which depends on the preamble

lengths and the pre-BF SNR. Then, given the variance of the combining phase errors, we approximate the distribution of the BF gains. The proposed framework is verified using simulations and experimentally using two BF software-defined radios (SDRs) in a lab environment. After deriving and verifying the framework, we consider two example design applications; one applicable to large swarms of small UAVs and the other for weather balloons. In the first example, for fixed BF overheads, we find the minimum number of BF radios to meet the required SNR. In the second example, for a fixed number of radios, we determine the shortest BF overheads that realize the SNR requirement. To the best of our knowledge, we are the first to demonstrate fully wireless distributed BF from flying UAVs without any wires attached. Our main contributions are:

- We proposed an analytical framework describing the relations between the BF gains and the pre-BF SNR, the length of the preambles, and the number of BF radios for a destination-led distributed BF protocol under the assumption of equal pre-BF SNRs. These relations were verified using simulations and experimentally using two BF software-defined radios.
- We characterized the distribution of BF gains assuming zero-mean normally distributed phase errors. We analytically derived a closed form expression for the variance of the BF gains. For large N , using central limit theorem, we proved that the BF gain distribution approaches Gaussian. For small phase error variance, using Taylor series, we approximated it using a Gamma distribution.
- Using the BF framework, we proposed approaches to determine the minimum number of BF radios and the shortest BF overheads to meet a required minimum post-BF SNR with a given probability. These approaches use mixed-integer convex optimization and bisection and were verified to meet the SNR requirements using simulations.

II. SYSTEM MODEL AND DISTRIBUTED BF PROTOCOL

A. System Model

Consider N identical radios collaborating to beamform a common payload to a destination radio D in a narrowband flat-fading channel. The BF radios can be remotely deployed Internet-of-Things devices communicating with a gateway or UAVs communicating with a ground station. The payload is encoded in the complex baseband signal $m(t)$ having unit power and it is assumed to be shared among the BF radios. The n -th radio transmits a signal $z_n(t)$ and the combined baseband signal at the destination is given by

$$y(t) = \sum_{n=1}^N a_n z_n(t) \exp\{j(2\pi f_n t + \phi_n)\} + w(t) \quad (1)$$

where between the destination and the n -th radio, a_n is the channel amplitude, f_n is the carrier frequency offset, and ϕ_n is the phase offset. The white Gaussian noise process is given by $w(t)$ and has power spectral density $N_0/2$. The phase and frequency offsets result from the lack of synchronization between the local oscillators of the radios, the wireless propagation

environment, and the Doppler frequency offsets resulting from the relative motion of radios. While these phenomena make the phase and frequency offsets time varying, we assume that the payload duration is shorter than the resulting channel coherence time and we approximate them as constant per payload.

For the signal $m(t)$ to combine coherently at the destination, the BF radios need to compensate for the phase and frequency offsets before transmission. The compensated signal transmitted by radio n , thus, is given by

$$z_n(t) = m(t) \exp\{-j(2\pi\hat{f}_n t + \hat{\phi}_n)\} \quad (2)$$

where \hat{f}_n and $\hat{\phi}_n$ are the n -th radio estimates of the frequency and phase offsets obtained through the BF protocol, which is described later. The received signal can be rewritten as

$$y(t) = m(t) \sum_{n=1}^N a_n \exp\{j\phi_n^e(t)\} + w(t) \quad (3)$$

where the combining phase error from radio n at instant t is given by

$$\phi_n^e(t) = (2\pi(f_n - \hat{f}_n)t + (\phi_n - \hat{\phi}_n)) \quad (4)$$

Due to residual frequency errors, the combining phase error increases with time and this makes the BF gains degrade with time. However, similar to most existing works in the literature, we only consider a single value for the BF gain per payload. To do that, we consider the evaluation instance to be t_e seconds after the start of phase estimation and we get $\phi_n^e = \phi_n^e(t_e)$. The beamforming gain at instant t_e can be defined as the ratio between the energy of the combined signals to that of the individual transmissions

$$G = \frac{\|\sum_{n=1}^N a_n \exp\{j\phi_n^e\}\|^2}{\sum_{n=1}^N a_n^2} \quad (5)$$

Each BF radio is assumed to transmit at its maximum power level P_T , which is common to all radios. We also assume that the BF radios experience similar signal attenuation, which would be the case if the radios are deployed in proximity of each other far from the destination. Given these assumptions, we get $a_n = a$ for all n , where a is the path loss. In that case, G becomes independent of path loss and simplifies to [27]

$$G = \frac{1}{N} \left| \sum_{n=1}^N \exp\{j\phi_n^e\} \right|^2 \quad (6)$$

which measures the gain for coherent combining that can take values up to N . The pre-BF SNR at the destination from one radio is given by

$$\gamma_{\text{preBF}} = \frac{a^2 P_T}{N_0} \quad (7)$$

and the post-BF SNR of the combined signal from all N BF radios is equal to

$$\gamma_{\text{postBF}} = NG\gamma_{\text{preBF}} \quad (8)$$

which considers both the gain from coherent combining (up to N) and increase in Tx power with the number of equal

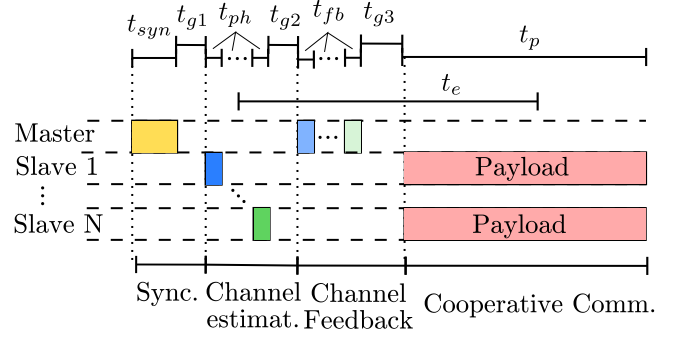


Fig. 1. Timing diagram of BF protocol. The destination is the master and BF radios are the slaves.

power radios (equal to N) and can be up to N^2 times the pre-BF SNR. The signals transmitted by the destination to the BF radios experience an SNR given by

$$\gamma_{\text{DR}} = \frac{a^2 P_T^D}{N_0} \quad (9)$$

where the destination has a transmit power P_T^D . The destination transmit power is assumed to be equal to or larger than that of the BF radios, which can be low power IoT devices or lightweight UAV mounted radios, i.e., $P_T^D \geq P_T$. Note that the post-BF SNR follows the same distribution of G , which we need to know to realize a minimum post-BF SNR with a given probability. As for G , it depends on ϕ_n^e , which results from the estimation errors during the BF protocol.

B. Beamforming Protocol

We start by describing the BF protocol, which aims to provide each BF radio with estimates of its phase and frequency offsets $\hat{\phi}_n$ and \hat{f}_n using the destination feedback. We consider a master-slave beamforming protocol [2], [7]; the destination radio is used as a master since it has a larger transmit power and the slaves are the beamforming radios. The master initiates the beamforming procedure and sends a preamble for frequency synchronization. After correcting their frequencies, the slaves send a channel estimation preamble to the master. The master calculates a phase estimate $\hat{\phi}_n'$ and transmits it back to the slaves that receive a slightly different value $\hat{\phi}_n$ due to feedback errors. Once each slave knows $\hat{\phi}_n$ and \hat{f}_n , they can start transmitting their payload.

In Fig. 1, we illustrate the transmitted signals. All the signaling is performed on the same frequency band, hence, all transmissions are received by all radios. The different beamforming stages can be described as follows

- 1) Synchronization: The master sends a synchronization (sync) preamble of duration t_{syn} . Using this signal each slave estimates its frequency offset \hat{f}_n . The time of arrival (TOA) of the sync preamble is used as a reference for timing at the slaves [28]. A guard time of duration t_{g1} is provided for the slaves to process the signals.
- 2) Channel Estimation: Each slave during a predetermined time slot sends a channel estimation preamble of duration t_{ph} . The master estimates $\hat{\phi}_n'$ from each slave. A guard time t_{g2} is used.

- 3) Channel Feedback: The master sends $\hat{\phi}'_n$ back to the slaves and due to feedback error each slave receives a slightly different phase estimate $\hat{\phi}_n$. A guard time t_{g3} is used.
- 4) Cooperative Communication: After estimating \hat{f}_n and receiving $\hat{\phi}_n$, all slaves adjust their signals accordingly and transmit their payload of duration t_p .

The duration of the BF overheads incurred by the protocol is given by

$$t_{ov} = t_{syn} + N(t_{ph} + t_{fb}) + t_{g1} + t_{g2} + t_{g3} \quad (10)$$

All the signal processing is assumed to be done in discrete time domain, hence all the time durations are assumed to be an integer multiple of the sampling time T_s . The time overhead can be written in terms of samples as

$$N_{ov} = N_{syn} + N(N_{ph} + N_{fb}) + N_{g1} + N_{g2} + N_{g3} \quad (11)$$

where N_{ov} is defined as $N_{ov} = t_{ov}/T_s$ and the remaining number of samples are defined similarly. As we can see from (11), the beamforming overheads scale linearly with the number of BF radios N . For short coherence time channels, the overheads N_{ov} are typically constrained, and to increase N while keeping N_{ov} constant, the duration of the preambles needs to be reduced. A few things to notice: (1) We assume that the payload is already shared among all the slaves. This can be achieved using a network broadcasting protocol [29], which we do not discuss in this work. (2) As for the guard time, it is dependent on the implementation of the BF protocol. A more optimized implementation using an FPGA for instance would require shorter guard times than an implementation using a general purpose processor. (3) Cooperative communication only requires the BF radios to be synchronized with each other and not necessarily with the destination. However, in order to use channel estimates from the destination, they need to be synchronized with the destination. (4) The BF protocol does not depend on our assumption of the BF radios having similar path loss. This assumption is only used in our analysis. (5) The time elapsed between the phase estimation and the evaluation time is larger for slave 1 than slave N , since each slave uses a different time-slot for phase estimation. To limit the error caused by this discrepancy, in our analysis, we consider t_e to start from the phase estimation slot of the middle slave as shown in Fig. 1 to the middle of the payload. The resulting error is negligible as long as $t_e \gg \frac{N}{2}t_{ph}$, which is the case as long the payload is longer than preambles as it is typically the case in practice. (6) Due to the time-slot base phase estimation, our analysis does not apply if the evaluation time t_e is chosen to correspond to the start of the payload ($t_e \gg \frac{N}{2}t_{ph}$ does not hold). However, evaluating the BF gain at the start of the payload does not represent the BF gain over the entire payload and does not have a practical importance.

Since BF is used to improve the SNR where the individual pre-BF SNR is low, the estimation errors within the protocol can not be neglected and will lead to a combining phase error ϕ_n^e as given by (4). At the evaluation time t_e , the variance of the combining phase error σ_e^2 defined as $\text{var}\{\phi_n^e\}$ under the assumption of independence of the three estimation errors is

given by

$$\sigma_e^2 = (2\pi t_e)^2 \sigma_f^2 + \sigma_{ph}^2 + \sigma_{fb}^2 \quad (12)$$

where the frequency estimation variance is given by $\sigma_f^2 = \text{var}\{f_n - \hat{f}_n\}$, the phase estimation and feedback variances are given by $\sigma_{ph}^2 = \text{var}\{\phi_n - \hat{\phi}_n\}$ and $\sigma_{fb}^2 = \text{var}\{\hat{\phi}'_n - \hat{\phi}_n\}$ respectively.

For the estimation of the time of arrival (TOA), after the detection of the sync preamble, correlation with a filter-bank is used for sub-sample-time accuracy as described in [16]. However, timing synchronization only affects intersymbol interference (ISI) at the destination without affecting the BF gains [2], so we do not discuss it in details.

In the following Sections (III and IV), we discuss the waveforms and estimators used for frequency estimation and phase estimation & feedback respectively. These estimators were chosen to have a low computational complexity suitable for an SDR implementation. We provide expressions for their error variances in terms of the pre-BF SNR and the preamble lengths. We argue that the resulting phase errors follow a zero-mean Gaussian distribution. For zero-mean Gaussian distributed phase errors with variance σ_e^2 , we approximate the distribution of the BF gain in Section V to complete the BF framework. This framework is numerically and experimentally verified in Section VI. After verifying the framework, we show how it can be used for designing BF systems in Section VII. The BF design procedures are illustrated using example scenarios in Section VIII.

III. FREQUENCY SYNCHRONIZATION

The objective of frequency synchronization is to eliminate the frequency offset between the destination and the BF radios. We start by discussing the signals used for synchronization and the proposed oneshot estimator and its variance. Then we discuss frequency tracking using Kalman filter assuming multiple successive BF cycles.

A. Frequency Offset Estimation

For frequency synchronization, we use a preamble consisting of N_{ZC} repetition of a Zadoff-Chu (ZC) sequence of length M similar to [16], satisfying $N_{syn} = N_{ZC}M$. The frequency estimator calculates the auto-correlation statistic

$$\eta_f = \sum_{m=0}^{N_{ZC}-2} \sum_{k=0}^{M-1} y_f^*[mM+k] y_f[(m+1)M+k] \quad (13)$$

where $y_f[k]$ is the noisy received preamble with the frequency offset, and $()^*$ denotes the conjugate operator. The frequency offset estimate at slave n is thus given by $\hat{f}_n = \frac{1}{2\pi T_s M} \angle \eta_f$ where $\angle(\cdot)$ denotes the phase of a complex number calculated using arctan. The term $\angle \eta_f$ calculates the phase difference between two successive sequence repetitions, under the assumption that M is small such that no phase wrapping occurs. The error variance for this estimator is given by [30, eq.70]

$$\sigma_{fe}^2 = \left(\frac{1}{M(N_{ZC}-1)^2 \gamma_{DR}} + \frac{1}{2M(N_{ZC}-1) \gamma_{DR}^2} \right) \frac{1}{(2\pi M T_s)^2} \quad (14)$$

TABLE I
KALMAN FILTER RELATIONS

Model	
$x_k = x_{k-1} + w_{k-1}$	(15)
$z_k = x_k + v_k$	(16)
Update	
$K_k = \frac{p_{k k-1}}{p_{k k-1} + r}$	(17)
$x_{k k} = x_{k k-1} + K_k(z_k - x_{k k-1})$	(18)
$p_{k k} = (1 - K_k)p_{k k-1}$	(19)
Predict	
$x_{k+1 k} = x_{k k}$	(20)
$p_{k+1 k} = p_{k k} + q$	(21)

This estimator is unbiased thus $\mathbb{E}\{\hat{f}_n - f_n\} = 0$ and was derived using a linear approximation of the arctan assuming η_f has a high SNR. By choosing M to be large, using the central limit theorem, the distribution of η_f can be approximated by Gaussian, thus making $\hat{f}_n - f_n$, which is approximated as linear in η_f , a zero mean Gaussian RV. However, at low SNR of η_f , $\angle\eta_f$ becomes uniform and the expression of σ_{fe}^2 no longer applies. This regime can be avoided by increasing N_{ZC} , otherwise, the BF gains will be too low to be of practical importance. Note that in practice the frequency offset is correlated among successive packets with short separation. This estimator, referred to as a oneshot frequency estimator, does not benefit from this correlation.

B. Interpacket Frequency Tracking Using Kalman Filter

If beamforming is performed periodically and the BF protocol is designed such that t_{cyc} is shorter than the channel coherence time, the frequency estimates between packets at each slave are correlated. Kalman filter (KF), thus, can be used to track the frequency to reduce the estimation variance. The drift system model and the KF equations are given in Table I for one BF radio following the conventional KF notation [31]. The frequency process drift and measurement models are given by (15) and (16), respectively, where x_k is the true frequency value in Hz (previously denoted by f_n) and z_k is the measured frequency at time kt_{cyc} . The noise terms for the process w_k and the measurement v_k are assumed to be zero mean Gaussian RV and their variances are q and r respectively. For the KF update equations, at step k , K_k is the Kalman gain, $x_{k|k-1}$ is the prediction of x and $p_{k|k-1}$ is the error variance given z_{k-1} . The value of $x_{k|k}$ is the predicted frequency offset and $p_{k|k}$ is its error variance given z_k .

By substituting (17) in (18) and using (20) we get

$$x_{k|k} = \frac{r}{p_{k|k-1} + r} x_{k-1|k-1} + \frac{p_{k|k-1}}{p_{k|k-1} + r} z_k \quad (22)$$

from which we can see that the KF creates a weighted average between the previous prediction and the current measurement. The weights of this average are based on the predicted process

variance $p_{k|k-1}$ and the measurement variance r . The larger the process variance relative to the measurement variance, the more weight is given to the measured value and vice versa. Since (22) is a linear equation, if z_k is a zero mean Gaussian RV, the output of KF will also be zero-mean and Gaussian. For BF, we are interested in calculating the KF error variance.

Proposition 1: The steady state frequency estimation error variance of KF from Table I is

$$\sigma_{fk}^2 = \frac{-q + q\sqrt{1 + 4\frac{r}{q}}}{2} \quad (23)$$

The proof is in Appendix A. Using (23) and assuming the system variances are accurately known, we argue that KF never increases the error variance. By rewriting (23), as $\sigma_{fk}^2 = \frac{-q + \sqrt{q^2 + 4qr}}{2}$, we can see that σ_{fk}^2 is non-decreasing in q and if $q = 0$, at convergence the error variance $\sigma_{fk}^2 = 0$ for any r . For $q \gg r$, r/q is small and using the approximation $\sqrt{1 + 4\frac{r}{q}} \approx 1 + 2\frac{r}{q}$, we get $\sigma_{fk}^2 = r$. Thus if q and r are perfectly known, the error variance reduction due to KF is higher for large r/q and, in the worst case scenario for small r/q , KF will give the measurement variance $\sigma_{fk}^2 = r$, as if we did not use KF. However, if the values of q and r used in KF do not match the system, this result does not hold and KF might deteriorate the frequency estimation. In practice, the value of r is the oneshot frequency estimator variance, which can be determined using an estimate of the SNR. The process variance q can be determined either using the oscillator datasheet [27] or empirically using measurements as described in [19]. Note that the extended KF (EKF) can track both phase and frequency and might yield a smaller variance than KF which only tracks the frequency. However, EKF can diverge due to phase wrapping [19], which is not desirable in a reliable BF system, and thus was not considered in this work.

IV. PHASE ESTIMATION AND FEEDBACK

The objective of the phase estimation and feedback is to have the slaves modify their signals to ensure coherent combining at the destination. In the phase estimation stage, each slave transmits a known signal $x_{ph}[n]$ consisting of N_{ph} samples. The master receives the noisy signal $y_{ph}[k]$. The proposed estimator calculates the correlation $\eta_{ph} = \sum_{k=0}^{N_{ph}-1} x_{ph}[k]^* y_{ph}[k]$, from which the phase estimate is calculated using $\hat{\phi}_n' = \angle\eta_{ph}$. The variance of this estimator can be calculated using [32, eq 9] as follows

$$\sigma_{phe}^2 = \frac{1}{2N_{ph}\gamma_{preBF}} \quad (24)$$

where $N_{ph}\gamma_{preBF}$ is the SNR of η_{ph} . The phase error $\hat{\phi}_n'$ follows a zero mean Gaussian distribution as long as the SNR of $\eta_{ph} \gg 1$ [32], which is the regime of interest.

As for the phase feedback, we use in-band feedback where the value of $\hat{\phi}_n'$ is encoded in the phase difference between two identical preambles to counter hardware phase ambiguity. Let the phase feedback preamble be given as a vector $\mathbf{x}_{fbp} \in \mathbb{C}^{N_{fb}}$. The master transmits the sequence

$$\mathbf{x}_{fb} = [\mathbf{x}_{fbp}^T \mathbf{x}_{fbp}^T e^{j\hat{\phi}_1'} \dots \mathbf{x}_{fbp}^T e^{j\hat{\phi}_n'} \dots \mathbf{x}_{fbp}^T e^{j\hat{\phi}_N'}]^T \quad (25)$$

Once received as $y_{fb}[k]$ with added noise, slave n estimates the phase difference between the first preamble and the n -th preamble using the statistic $\eta_{fb} = \sum_{k=0}^{N_{fb}-1} y_{fb}[k]y_{fb}[k + nN_{fb}]$ and calculates the angle $\hat{\phi}_n = \angle \eta_{fb}$. The variance of the feedback is similar to that used for frequency estimation in (14) (with $N_{ZC} = 2$, $M = N_{fb}$) and is given by

$$\sigma_{f_{be}}^2 = \left(\frac{1}{N_{fb}\gamma_{DR}} + \frac{1}{2N_{fb}\gamma_{DR}^2} \right) \quad (26)$$

Note that there are other ways to feedback the phase estimates, however, this approach is simple to implement. Another alternative was to encode the values of $\hat{\phi}'_n$ as floating-point numbers and transmit them using digital modulation. However, since we are considering a low SNR and a mistake in one of the most significant bits can be detrimental, we would need to implement channel coding. This would add unnecessary complexity to our protocol. Also note that the error variance of proposed estimators in this section are derived assuming zero residual frequency errors ($f_n - \hat{f}_n$). In practice, frequency estimation errors would increase the variance of phase estimation and feedback. However, the impact of ($f_n - \hat{f}_n$) is negligible on σ_e^2 and $\sigma_{f_{be}}^2$ compared to $(2\pi t_e)^2 \sigma_f^2$ under the assumption that $t_e \gg t_{ph}$ and $t_e \gg t_{fb}$.

V. BEAMFORMING GAIN ANALYSIS

In this section, our objective is to approximate the distribution of G , assuming that the ϕ_n^e are independent Gaussian random variables (RVs) with zero mean and variance σ_e^2 . The Gaussian assumption applies to our protocol because the errors of the proposed estimators are independent and can be approximated by a zero-mean Gaussian RVs. Hence, their sum according to (4) is also zero-mean Gaussian. We start by calculating the mean and variance of the distribution.

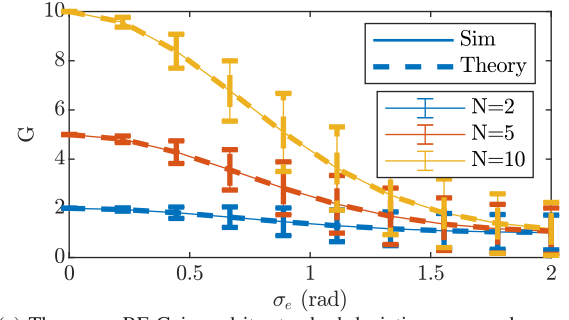
Proposition 2: For signals combining from N radios having independent zero mean Gaussian phase with variance σ_e^2 , the mean and the variance of the BF gains G are given by

$$\mathbb{E}\{G\} = 1 + (N-1)e^{-\sigma_e^2} \quad (27)$$

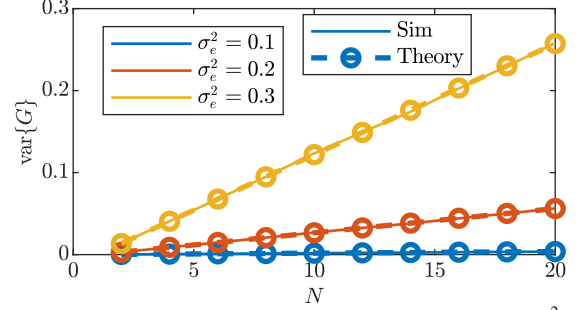
$$\text{var}\{G\} = \frac{(N-1)}{N}(1 - e^{-\sigma_e^2})^2 \left((1 - e^{-\sigma_e^2})^2 + 2Ne^{-\sigma_e^2} \right) \quad (28)$$

The proof is in Appendix B. Note that the mean was previously derived in [27]. In Fig. 2a, we plot the average BF gain using (27) as a function of σ_e with the error bars representing the standard deviation ($\sqrt{\text{var}\{G\}}$). For $\sigma_e = 0$, we get a BF gain of N as we ideally expect. As σ_e increases, the mean BF gains decrease and their variances increase and this happens faster for larger N . Thus when designing a BF system unless N and σ_e are small, we can not assume a perfect N fold power increase due to BF. To verify the derived mean and variance, for each value of N and σ_e , we sampled 100,000 zero mean Gaussian RVs of variance σ_e^2 for each radio and added them to calculate G numerically. The simulations shown in Fig.2a as thick dashed lines with dashed error bars overlap the derived expressions verifying Proposition 2.

To better understand the variance behavior with N , for small σ_e^2 , we simplify (28) to get $\text{var}\{G\} \approx 2Ne^{-\sigma_e^2}(1 - e^{-\sigma_e^2})^2$.



(a) The mean BF Gain and its standard deviation as error bars.



(b) The relation between the BF variance and N for fixed σ_e^2 .

Fig. 2. The relation between BF gain, N , and σ_e^2 .

Thus the variance increases linearly with the number of slaves for small σ_e^2 . The linear relation between $\text{var}\{G\}$ and N is illustrated in Fig.2b. The higher the value of σ_e^2 , the larger the slope. The large discrepancy in the values of the variance with N shows the importance of considering the distribution of G and not just its mean in the design of reliable BF systems. Next, we approximate the distribution of G . First, we consider the case of large N using the central limit theorem. Then, we consider the case for a small N and small σ_e^2 and use the Taylor series to derive the approximation.

Proposition 3: For large N , the distribution of G tends to a Gaussian distribution with mean and variance given by Proposition 2.

Proposition 4: For small combined phase error variance σ_e^2 or for large N , the distribution of G can be approximated by $N - X_\gamma$ where X_γ is a random variable following the Gamma distribution $X_\gamma \sim \Gamma(K, \theta)$ with

$$K = \frac{N(N-1)}{(1 - e^{-\sigma_e^2})^2 + 2Ne^{-\sigma_e^2}} \quad (29)$$

$$\theta = \frac{1}{N}(1 - e^{-\sigma_e^2}) \left((1 - e^{-\sigma_e^2})^2 + 2Ne^{-\sigma_e^2} \right) \quad (30)$$

The proofs are in Appendices C and D respectively. We start by plotting the empirical cumulative distribution function (CDF) of G for small N and a small $\sigma_e = 0.1$ in Fig. 3a. We can see that the distribution is not Gaussian and is accurately approximated by the Gamma distribution. Then, we consider a large $N \geq 30$ and relatively large value of $\sigma_e = 1$ in Fig. 3b. From that Figure, we can see that all three CDFs overlap for large N and large σ_e verifying Prop. 3 and 4. Based on these results, since the Gamma distribution applies to a wider range of N and σ_e^2 , we use it later to approximate the BF gain distribution. Note that neither approximation is

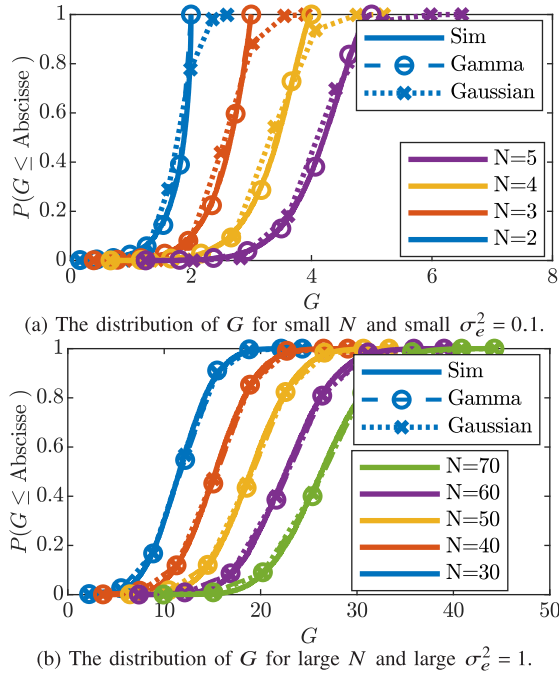


Fig. 3. The distribution of G for different N and σ_e^2 .

accurate for small values of N and a large value of σ_e^2 , however, in this regime the BF gains are small with a large variance, which is not of practical importance. It is important to note that the derived variance and distribution approximation in this section apply to any BF protocol where the phase error ϕ_n^e is independent for all n and can be approximated by zero-mean Gaussian RVs. For our protocol, the value of σ_e^2 can depend on N for scenarios where the BF overhead N_{ov} is constrained by the channel coherence time. In such scenarios, the duration of each preamble decreases as N increases to satisfy the fixed N_{ov} . Thus the estimators error variances and consequently σ_e^2 increase with N . The dependence between N and σ_e^2 is considered when designing the BF preambles in short coherence channels later in Section VIII-A.

VI. NUMERICAL AND EXPERIMENTAL VALIDATION

In this Section, after deriving the BF framework, we verify it numerically and experimentally and we show that it can be used to predict the BF gains at different SNRs. Using UAV experiments and emulation over a UAV channel trace, we evaluate the impact of the channel coherence time on the BF gains.

A. Numerical Validation

We simulated the BF protocol between a destination radio and N BF radios. During a BF cycle, signals transmitted from BF radio n to the destination is multiplied by $e^{j(2\pi f_n t + \phi_n)}$ with noise added to realize the SNR γ_{preBF} . Any signal transmitted the other way uses the negative value of f_n with noise added to realize the SNR γ_{DR} . At the start of each BF cycle, for BF slave n , we sample uniform random phase ϕ_n and f_n is generated using a discrete Wiener process as

TABLE II
BEAMFORMING WAVEFORM SPECIFICATIONS

Scenario	Parameters
Simulation	$N_{ZC} = 10, M = 63, t_{syn} = 0.63ms, t_{ph} = 0.1ms, t_{fb} = 0.1ms, t_{g1} = t_{g2} = t_{g3} = 1ms, t_p = 12ms, t_e = 9ms, t_{cyc} = 50ms$
Lab	$N_{ZC} = 10, M = 63, t_{syn} = 0.63ms, t_{ph} = 0.1ms, t_{fb} = 0.1ms, t_{g1} = 6ms, t_{g2} = 4ms, t_{g3} = 16ms, t_p = 10ms, t_{cyc} = 180ms$
UAV	$N_{ZC} = 10, M = 63, t_{syn} = 0.63ms, t_{ph} = 0.1ms, t_{fb} = 0.1ms, t_{g1} = 6ms, t_{g2} = 4ms, t_{g3} = 11ms, t_p = 1ms, t_{cyc} = 75ms$

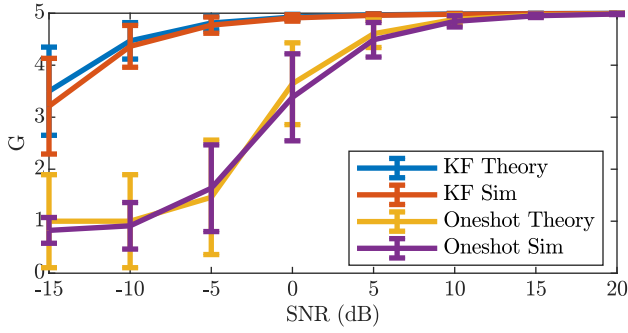
described in (15) having variance q . Since we are assuming that the signal is transmitted within the channel coherence time, both frequency and phase are assumed to be constant during the same BF cycle.

The signals transmitted follow the BF protocol. For phase estimation and feedback, we used the estimators discussed in Section IV and for frequency offset we either used the oneshot estimator from Section III-A alone or combined with KF. To avoid errors in measuring the BF gain, the combined signal magnitude was evaluated at time t_e before adding the noise.

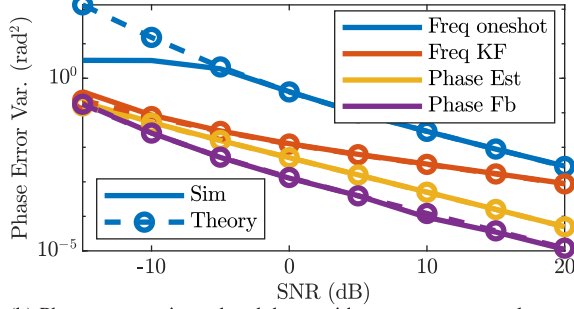
In our simulations, we considered $N = 5$ BF radios using a sampling rate of 1MHz ($T_s = 1\mu s$). At this sampling rate, since a typical near-urban air-to-ground channel has a median root-mean-square delay spread of 11ns ($\ll 1\mu s$) [33], the narrowband flat-fading channel assumption is justified. The exact duration of each preamble is given in the first row of Table II and we used $q = 0.18$. The evaluation time $t_e = 9ms$ is in the middle of the payload. One million BF cycles were simulated.

We start by discussing the results obtained when using the oneshot frequency estimation. The average BF gain obtained from simulations is plotted in Fig. 4a with the error bars representing its standard deviation. For the oneshot results, the theoretical value is obtained by calculating the variance of each estimator using (14), (24), and (26), calculating σ_e^2 using (12), then the BF gain mean and variance using Proposition 2. From that Figure, we can see that the theoretical mean matches the simulations to a large extent. As for the variances, they match except for SNRs below 0dB. By plotting a breakdown of the phase error for the slave $n = 3$ using (12) in Fig. 4b, we see that at SNRs below 0dB the theoretical oneshot frequency variance is overestimated. This happened because the phase error becomes uniform and the Gaussian assumption no longer holds leading to the discrepancy in Fig. 4a. At these low SNRs, the BF gains are negligible and this is not a useful BF design. From Fig. 4b, since the phase error from the frequency estimation error is dominant, it would be beneficial to allocate more time to frequency estimation or use the KF to reduce its variance.

Next, we discuss the BF results when using KF using the same Figures 4a and 4b. The theoretical KF variance is calculated using (23) with the measurement variance r being the oneshot variance and q perfectly known. From Fig. 4a,



(a) BF Gains using oneshot and KF for frequency synch. The standard dev. is shown as error bars.



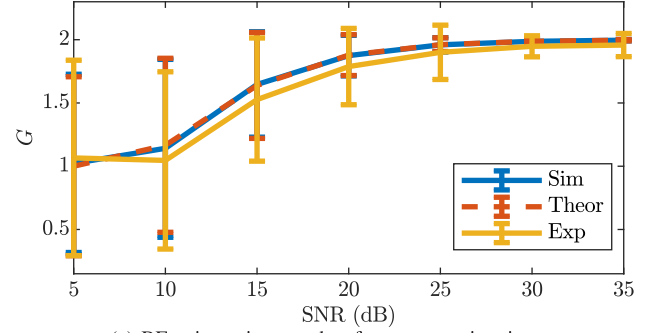
(b) Phase error variance breakdown with respect to protocol stages.

Fig. 4. Simulated BF Gains and phase errors at different SNRs for $N = 5$ using the waveform from Table II.

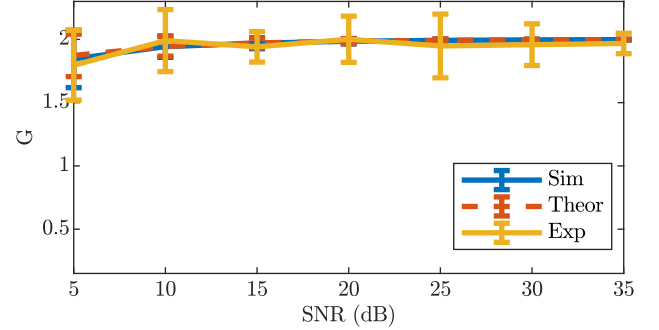
we can see that both theoretical and simulated curves overlap. A small discrepancy exists at low SNR, which we attribute to an insufficient number of BF cycles. Since KF is a recursive filter, its output depends on all previous cycles and convergence is slower for high measurement noise variance [34]. Compared to the oneshot BF, at low SNR, KF provides significant BF gain improvements by reducing the frequency estimation variance and the resulting phase errors as shown in Fig. 4b. From that Figure, we also see that as the SNR (above 0dB) becomes larger, the gap between oneshot and KF decreases. This happens because as r decreases at high SNR, the ratio r/q becomes small and the benefit from using KF decreases.

B. Experimental Validation

The proposed BF protocol was implemented using three USRP B205-mini software-defined radios (SDR); two were used as BF radios and one as the destination radio. The destination radio initiates a BF cycle by transmitting the frequency synchronization preamble. The BF radios are always running the autocorrelation given by (13) and using its output power level to detect the preamble. Once detected, the frequency offset is estimated (using oneshot or KF) and corrected. Each BF radio transmits the phase estimation preamble in a preassigned time slot. The destination radio estimates the phase and feeds it back to the BF radios using the same previously discussed waveforms and estimators. Once the feedback is obtained, the radios transmit a known payload, which is received and stored by the destination. The timing of the phases estimation, feedback, and payload was implemented



(a) BF gains using oneshot frequency estimation.



(b) BF gains using KF for frequency estimation.

Fig. 5. Experimental results collected using $N = 2$ BF software-defined-radios in a lab along with the theoretical results predicted by the BF framework and simulations.

using the USRP hardware driver (UHD) timing tags in reference to the sync preamble. The payload consists of three parts; each of the two BF radio transmits individually at first, then both BF radios transmit simultaneously. The magnitude of each part of the payload is estimated by averaging, then the BF gain is calculated by dividing the power of the simultaneous transmission by the sum of the individual transmissions as per (5). All the signal processing was implemented using GNUradio [35] and timed burst transmissions were used for the different stages of the protocol. The destination processing was performed on a laptop and the BF radios on ODROID XU4 single board computers (SBC). We conducted the experiments in the lab and on UAVs at a frequency of 915MHz with a sampling period of $T_s = 1\mu s$.

1) *Lab Experiment*: We started by verifying our simulations on a small scale in a lab environment with a favorable channel. The BF radios were placed in proximity from each other to experience similar path loss as assumed in our analysis. The destination was 2.5 meters away from the radios in an undisturbed line-of-sight environment with a measured coherence time of $0.3s^1$ and $q = 0.18$. Both the destination and BF radios were set to use the same transmit gain, which was varied in increments of 5dB to obtain different SNRs. At each SNR, 900 beamforming cycles were performed. The timing of the protocol is shown in Table II. Notice that the guard times are much longer than in the simulations to allow the

¹The coherence time was calculated as the time that satisfies $|R(\tau_c)| = R_L$ [36] where $R(t)$ is the normalized channel correlation obtained through measurements, and $R_L = 0.5$ is the coherence level.

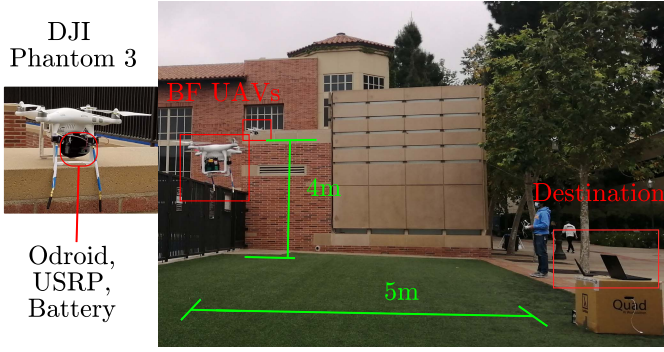


Fig. 6. The UAV experiment consists of 2 BF UAVs with SDRs mounted on-board. The UAVs were hovering freely and were not attached to the ground by wires.

TABLE III
BF UAV RESULTS

Setup	Freq	SNR (dB)	G Mean	G Stdev
Ground	KF	26.9	1.825	0.319
Flying	oneshot	23.7	1.636	0.525
Flying	KF	24.9	1.632	0.438

BF signal processing to operate in real-time, which makes t_e larger in (4), and thus increases σ_e^2 and degrades the BF gains.

The experimental results along with its simulated and theoretical equivalents are shown in Fig. 5a. We can see that the measured results are close to the simulation and theoretical results, which overlap. The improvement from using KF follows a similar trend to what was observed in Fig. 5b. This result experimentally verifies our simulation setup and analysis.

2) *UAV Experiment*: Next, we move our setup from the lab to UAVs. The BF radios, consisting of the SBC and USRPs along with a battery, were mounted on two DJI Phantom 3 drones as shown in Fig. 6. The destination radio was placed on the ground about 5m away from the UAVs which flew at a height of about 4m. The wind speed at the day of the experiment was 15Km/hr. Due to the wind and the noise of the UAV sensors, the UAVs were not stable and drifted within about a meter. The UAV operators frequently intervened to stabilize them.

Based on channel estimation performed before the experiment, the coherence time was estimated to be about $\tau_c = 85ms$. Thus, the lab experiment BF cycle ($t_{cyc} = 180ms$) is too long for the UAV channel. For the BF to work from the UAVs, the BF cycle was redesigned to have shorter guard times and a 10 times shorter payload as detailed in Table II, yielding a reduced $t_{cyc} = 75ms$, which is shorter than τ_c but only with a small margin. The experiment was performed with three settings: 1) UAVs were on the ground and used KF for frequency synchronization, 2) UAVs were flying and used oneshot for frequency synchronization and 3) UAVs were flying and used KF. The BF results are shown in Table III along with the average SNR. The BF UAVs attained about 80% of the ideal BF gains despite the low coherence time channel.

TABLE IV
BF EMULATION OVER UAV CHANNEL TRACE

#	SNR	t_{cyc}	τ_c	KF σ_e^2 [G]	Onesh. σ_e^2 [G]
1	24dB	75ms	85ms	0.569 [1.725]	0.567 [1.723]
2	24dB	18ms	85ms	0.11 [1.99]	0.141 [1.98]
3	0dB	18ms	85ms	0.573 [1.85]	0.4 [1.72]

These gains are lower than the ground scenario as expected because of the shorter coherence time. As for the comparison between KF and oneshot, there is no significant difference because r/q is small; r is small because of the high SNR and q is large because of the short coherence time.

C. Emulation

To overcome the large delays of the BF implementation and have a fair comparison between KF and Oneshot, we emulated BF over a channel trace. The channel trace was obtained by capturing a repeating ZC sequence from a flying UAV over a period of 100s. Using this trace, we emulated the BF protocol as follows; we used a duration t_{syn} to estimate the frequency offset and corrected for it, then we estimated the phase offset after a delay equivalent to the protocol ($t_{g1} + Nt_{ph} + t_{g2}$) and corrected for it. The feedback stage was not emulated and was assumed to be ideal. At the evaluation time t_e , we estimated the phase error ϕ^e which for a static channel and perfect estimation should equal zero. The variance of ϕ^e calculated by emulation over the entire trace provides an estimate of σ_e^2 if BF was applied in this channel. Note that the channel trace was collected over one capture with a USRP operating in half-duplex. Hence, the emulation over that trace does not capture distortions due to burst transmissions and having both transmit and receive chains powered on simultaneously in the protocol implementation.

The measured phase errors are reported in Table IV. The first row emulates the timing used in the UAV experiment and using the value of $\tau_c = 85ms$, which is the true one, to calculate the KF q . The calculated phase error variance σ_e^2 is shown for KF and oneshot, and the theoretically predicted mean BF gain G using (27) and $N = 2$. Due to the more favorable half-duplex capture and the ideal feedback, the predicted emulation BF gains (≈ 1.7) are better than the measured ones (≈ 1.6). For the relatively long BF packets at a the high SNR of the capture, the predicted BF gains using both oneshot and KF are very close (1.725 and 1.723) similar to our experimental results. Yet the BF gains are still below 2 due to the long BF cycle, so in row 2, we emulate the protocol using a shorter cycle of 18ms by scaling down t_e and the phase delay. Using this shorter cycle, the BF gains increase significantly for both KF and oneshot and approach the ideal gain of 2. This is the result we would expect using an optimized implementation of the BF protocol having shorter guard times. Due to the high SNR, both KF and oneshot still give a similar performance. Then in row 3, we added Gaussian noise to the channel trace to make its SNR drop to 0dB. The expected BF gains for KF become significantly better than

those from oneshot. This result shows that if we designed the BF protocol such that $t_{\text{cyc}} \ll \tau_c$, KF can attain significantly higher BF gains than oneshot for distantly deployed UAVs.

VII. BEAMFORMING SYSTEM DESIGN

After verifying the framework, we discuss how it can be used in designing BF systems. To design a reliable BF system, we need to specify the number of BF radios N and the duration of the preambles to exceed a minimum post-BF SNR with a given probability. The design procedure is over two steps; first we determine N and σ_e^2 that meet the requirements and then we design the preambles' lengths to realize σ_e^2 at a given pre-BF SNR. Later in Section VIII, we apply the proposed design procedures for specific scenarios.

A. Specifying N and σ_e^2

Although the pre-BF SNR (γ_{preBF}) is assumed constant, due to the phase error variance, the post BF SNR (γ_{postBF}) varies randomly. A reliable BF system has to exceed a specified outage probability p_{out} such that $P(\gamma_{\text{postBF}} < \gamma_{\text{min}}) \leq p_{\text{out}}$, where γ_{min} is the required minimum SNR. Using the gamma approximation of the BF gain distribution and the post-BF SNR definition (8), we can rewrite $P(\gamma_{\text{postBF}} < \gamma_{\text{min}}) = 1 - F_{X_\gamma} \left(N - \frac{\gamma_{\text{min}}}{\gamma_{\text{preBF}} N} \right)$ where $F_{X_\gamma}(x)$ is the CDF of the Gamma distribution from Proposition 4 whose mean and variance depend on N and σ_e^2 . Hence, our objective is to determine N and σ_e^2 which satisfy

$$F_{X_\gamma} \left(N - \frac{\gamma_{\text{min}}}{\gamma_{\text{preBF}} N} \right) \leq 1 - p_{\text{out}} \quad (31)$$

We know the distribution of X_γ and how N and σ_e^2 affect it, however, inverting (31) to obtain an explicit relation between N and σ_e^2 is intractable. The fact that σ_e^2 can depend on N under fixed BF overheads further complicates analytical solutions. It is easy, however, to check whether a given choice of N and the corresponding σ_e^2 satisfies the requirements given by (31). Thus, we resort to numerical trial-and-error methods to find N and σ_e^2 satisfying the requirements. The exact method depends on the scenario and whether N is fixed or not, and thus its discussion is deferred to Section VIII where example scenarios are presented.

B. Beamforming Signals Design

For given values of N , γ_{preBF} , and γ_{DR} , we want to optimize the time allocated to each preamble for σ_e^2 to meet the system requirements. We identify two problems of interest; the first one is to minimize σ_e^2 for bounded BF overheads. This problem formulation is suited for short coherence time channels (relative to the payload), where the BF overheads are constrained. In Sec. VIII-A, we use this formulation to find the minimum number of BF radios meeting an SNR requirement in a short coherence time channel. The second problem is to minimize the BF overheads N_{ov} to meet a maximum allowable phase error variance. This problem is suited for relatively large coherence time channels, where large BF overheads are possible. In Sec. VIII-B, for a fixed N ,

we use this formulation to find the minimum BF overhead that meets an SNR requirement in a large coherence time channel.

Next, we formulate both problems. The total overheads in samples defined in (11) can be written as a function of the duration of each stage $N_{\text{ov}}(N_{\text{syn}}, N_{\text{ph}}, N_{\text{fb}})$. For fixed N , γ_{preBF} and γ_{DR} , the phase variance σ_e^2 becomes a function of the number of samples allocated to each stage $\sigma_e^2(N_{\text{syn}}, N_{\text{ph}}, N_{\text{fb}})$ defined as

$$\sigma_e^2(N_{\text{syn}}, N_{\text{ph}}, N_{\text{fb}}) = (2\pi t_e)^2 \sigma_f^2(N_{\text{syn}}) + \sigma_{ph}^2(N_{\text{ph}}) + \sigma_{fb}^2(N_{\text{fb}}) \quad (32)$$

The values of σ_f^2 , σ_{ph}^2 , and σ_{fb}^2 are dependent on the choice of estimators and are a function of N_{syn} , N_{ph} , and N_{fb} respectively. For our choice of estimators $\sigma_{ph}^2 = \sigma_{phe}^2$ defined by (24), and $\sigma_{fb}^2 = \sigma_{fbe}^2$ defined by (26). As for the frequency error variance, if we use oneshot estimation $\sigma_f^2 = \sigma_{fe}^2$ as defined by (14) and if we use the KF $\sigma_f^2 = \sigma_{fke}^2$ as defined by (23) with $r = \sigma_{fe}^2$.

Note that for a chosen Zadoff-Chu sequence of a length M , we can only optimize the number of repetitions N_{ZC} to change N_{syn} . Hence, for fixed N , the problem P1 can be written as

$$P1 : \underset{N_{\text{ZC}}, N_{\text{ph}}, N_{\text{fb}}}{\text{minimize}} \sigma_e^2(N_{\text{ZC}}M, N_{\text{ph}}, N_{\text{fb}}) \quad (33)$$

$$\text{subject to } N_{\text{ov}}(N_{\text{ZC}}M, N_{\text{ph}}, N_{\text{fb}}) \leq \delta_{N_{\text{ov}}} \\ N_{\text{ZC}}, N_{\text{ph}}, N_{\text{fb}} \in \mathbb{Z}^+, N_{\text{ZC}} \geq 2 \quad (34)$$

where $\delta_{N_{\text{ov}}}$ is maximum overhead length which depends on the channel coherence time, and \mathbb{Z}^+ is the set of positive integers. For a maximum allowable phase error $\delta_{\sigma_e^2}$, the second problem P2 can be written as

$$P2 : \underset{N_{\text{ZC}}, N_{\text{ph}}, N_{\text{fb}}}{\text{minimize}} N_{\text{ov}}(N_{\text{ZC}}M, N_{\text{ph}}, N_{\text{fb}}) \quad (35)$$

$$\text{subject to } \sigma_e^2(N_{\text{ZC}}M, N_{\text{ph}}, N_{\text{fb}}) \leq \delta_{\sigma_e^2} \\ N_{\text{ZC}}, N_{\text{ph}}, N_{\text{fb}} \in \mathbb{Z}^+, N_{\text{ZC}} \geq 2 \quad (36)$$

Then, we argue that for our choice of estimators, both problems are convex with respect to their variables and thus are easy to solve. Except for the KF, all these estimators take the form $f(x) = \frac{c_1}{x} + \frac{c_2}{x^2}$ with respect to their variables for some positive c_1 and c_2 where x is strictly positive, hence they are all convex over their domain. As for the KF, when substituting for r , it takes the form $f(x) = c_1 + \sqrt{c_2 + \frac{c_3}{x} + \frac{c_4}{x^2}}$ with respect to its positive variable x for some positive c_1, c_2, c_3 and c_4 . This can be rewritten as $f(x) = c_1 + \|\mathbf{y}\|$ where $\mathbf{y} = [\sqrt{c_2}, \frac{\sqrt{c_3}}{\sqrt{x}}, \frac{\sqrt{c_4}}{x}]^T$. The norm is convex and non decreasing and $\frac{\sqrt{c_3}}{\sqrt{x}}$ and $\frac{\sqrt{c_4}}{x}$ are convex for positive x . By applying the composition rule [37], the KF variance is convex. Hence, $\sigma_e^2(N_{\text{ZC}}M, N_{\text{ph}}, N_{\text{fb}})$ is convex with respect to its arguments for all of our estimators. As for $N_{\text{ov}}(N_{\text{ZC}}M, N_{\text{ph}}, N_{\text{fb}})$, it is an affine combination of its arguments. This makes both problems P1 and P2 integer convex problems, which can be optimally solved using CVX with a mixed integer solver [38].

VIII. BEAMFORMING DESIGN SCENARIOS

The proposed BF framework and the derived relations can be applied to many BF scenarios. In this section, we discuss

the design procedures for two example scenarios. In the first example, we consider a large swarm of small UAVs; we want to determine the minimum N to satisfy the SNR requirements. Due to the UAVs' high mobility, the channel coherence time is small and the BF overheads are constrained. This example maps to the problem P1. In the second example, we consider $N = 4$ weather balloons sending short payloads. Due to the long coherence time resulting from the balloons slow motion, large BF overheads are possible. However, to avoid energy wasted on unneeded transmission, our objective is to minimize the BF overheads while satisfying the SNR requirement. This example maps to the problem P2.

A. Swarm of Small UAVs

A swarm of N_{ub} small UAVs is deployed in an urban environment for an application like crowd monitoring [39]. A large number of small UAVs is deployed and they continuously transmit data. To avoid a large overhead in data sharing among UAVs for BF, we want to determine the minimum number of UAVs to beamform such that the destination SNR exceeds a minimum of $\gamma_{min} = 5dB$ for 90% of the time ($p_{out} = 0.1$).

For the urban channel, we consider a channel having a path loss coefficient of 3.7 [40] and a coherence time of 10ms [41]. The maximum transmit power of each UAV is $P_T = 0dBm$ and of the destination $P_T^D = 20dBm$. Communication takes place over a frequency of 915MHz using a sampling time of $T_s = 1\mu s$ and a BW of 1MHz and all radios have a noise figure of 3dB. By performing the link budget calculation, the SNR from an individual UAV at 1Km is close to $-13dB$, so the minimum required SNR improvement due to BF is $G_{req} = 18dB$. Assuming ideal BF yielding an SNR improvement of N^2 , only 8 BF radios are required. However, due to the short coherence time, the entire BF packet is assumed to be limited to 5ms and based on the payload required by the application only 1ms of BF overhead is allowed. At this low SNR and with this short BF overhead, the ideal beamforming gains are not achievable and large BF variance is expected. We need to use more than 8 BF radios so that the SNR exceeds 5dB for 90% of the time as required. Our objective is to determine the minimum N and the duration of each preamble.

We use our analytical framework to find the minimum N . Since for fixed overheads N_{ov} , σ_e^2 depends on N , we need to solve P1 to calculate σ_e^2 for each N . The proposed approach is summarized in Algorithm 1 and it works as follows; we start from the lower bound on N , which occurs when assuming ideal BF $N_{lb} = \lceil \sqrt{G_{req}} \rceil$ and increment N until the requirement is satisfied. For each N , we solve the minimum phase error problem P1 to obtain σ_e^2 . Using the resulting σ_e^2 , we substitute in (31) to determine if the requirement is satisfied or not. The first N satisfying the requirement is the minimum N meeting the SNR requirements. If the maximum number of available BF radios N_{ub} was reached without satisfying (31), another approach needs to be considered to meet the requirements like increasing the BF overhead or the transmit power of the radios. Since the BF is performed periodically and $t_{cyc} < \tau_c$, we assume that KF is used for frequency tracking.

Algorithm 1 Solving for minimum N

```

input :  $N_{lb}, N_{ub}, N_{ov}, p_{out}, \gamma_{min}$ 
output: Solved,  $N$ ,  $N_{syn}, N_{ph}, N_{fb}$ 
Set Solved = False ;
for  $n_i = N_{lb}$  to  $N_{ub}$  do
    Solve P1 to determine  $N_{syn}, N_{ph}, N_{fb}, \sigma_e^2$ ;
    if  $n_i$  and  $\sigma_e^2$  satisfy (31) then
        Set Solved = True; Set  $N = n_i$ ; Exit ;
    end
end

```

The calculated N for different distances is shown in Fig. 7a along with N_{lb} calculated assuming ideal BF gain. To verify that the obtained solution meets our design criteria, we simulated 10K BF cycles of the BF protocol using the calculated N and the optimized waveforms obtained from P1 at each distance. The destination SNR was measured and its empirical CDF for the proposed N and the ideal N_{lb} are plotted in Fig. 7b and 7c respectively. From these Figures, we see that the required outage probability is met using the proposed N . Thus, our problem solution and the underlying analysis can be used to design reliable BF systems satisfying the design requirements as verified by simulations. On the other hand, relying on the ideal N_{lb} is expected to yield lower BF gains than the desired ones in realistic deployment scenarios.

Looking at Fig. 7a, we observe an interesting trend. For the calculated N , the number of BF radios increases by 10 from 1KM to 1.1KM compared to only 4 from 900m to 1Km, in contrast to ideal BF (N_{lb}), where number of BF radios increase by a fixed rate of 1 radio. This faster rate of increase is caused by the increasing number of exchanged signals associated with the larger N and the decreasing pre-beamforming SNR; to maintain fixed BF overheads, using more radios corresponds to shorter preambles, which in turn leads to degraded BF gains. Similarly, the pre-beamforming SNR decreases with distance, which further degrades the BF gains. Thus more BF radios are needed to counter the degrading BF gains. This trend and the minimum needed N cannot be trivially predicted from N_{lb} . For example using $N_{lb} + 5$ or using $1.2N_{lb}$ will not yield the proposed N for all distances and might result in using too many or too few radios. This further justifies the need for our design framework.

B. Weather Balloons

Weather balloons are deployed at high altitudes to perform atmospheric measurements and report them back to the ground. We consider $N = 4$ weather balloons deployed at a distance of 50KM from the destination radio. Due to their high altitude, the channel is dominated by line-of-sight propagation and we consider a path loss coefficient of 2 and a large channel coherence time exceeding 100ms. The large channel coherence time allows for much longer BF overheads. However, to economize the balloon payload battery power, we want to minimize the transmission time. Our objective is to determine the smallest BF overheads to attain a received

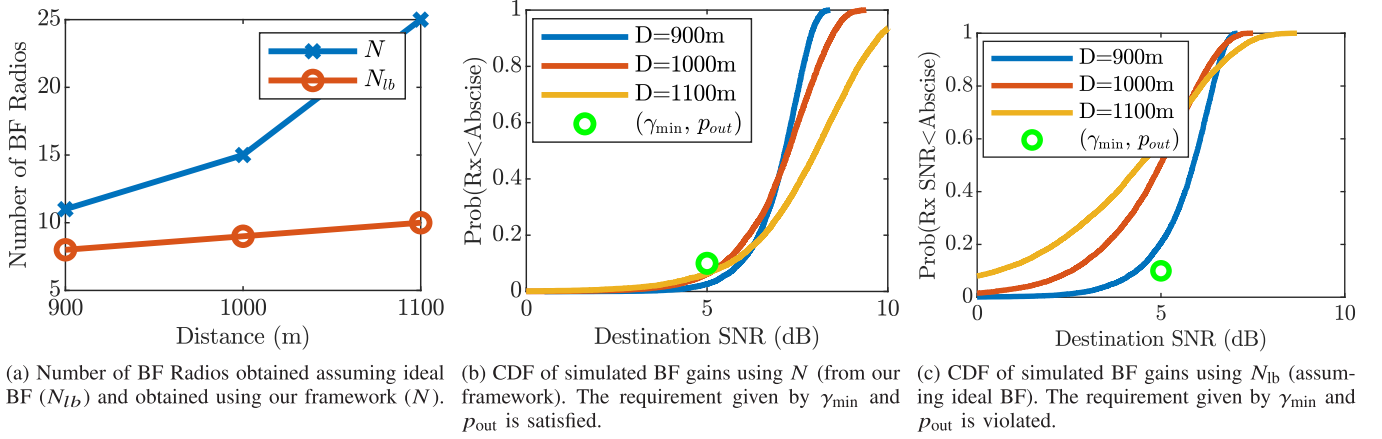
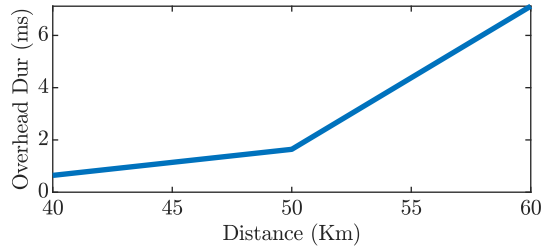
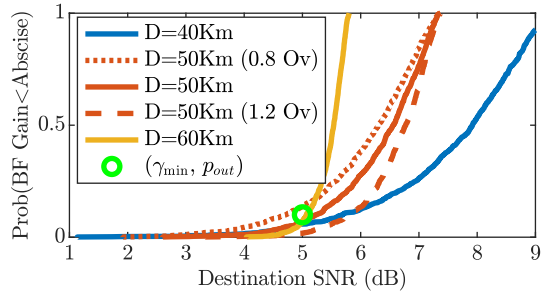


Fig. 7. Results for minimizing N in a swarm of small UAVs assuming a fixed BF overhead. Using N obtained from our approach, the SNR requirement is satisfied as verified by simulations.



(a) The minimum BF overhead to satisfy the SNR requirement.



(b) CDF of simulated BF gains. The SNR requirements (γ_{min}, p_{out}) are met when using the minimum overhead (Ov) in solid. For 50 Km, the requirements are not met when using 0.8 Ov and are exceeded for 1.2 Ov.

Fig. 8. For $N = 4$ weather balloons, in a long coherence time channel, the minimum overheads (Ov) obtained using our framework satisfy the SNR requirements. Shorter Ov violate requirements and longer Ov exceed them.

SNR exceeding a minimum of $\gamma_{min} = 5dB$ for 90% of the time ($p_{out} = 0.1$). We use the same power, frequency, bandwidth, and noise parameters as the previous scenario except $P_T = 10dBm$ is larger. The SNR from a single radio is $-4.6dB$ and thus the required BF gain at 50KM distance is $9.6dB$. Assuming that the measurements are infrequent and not periodic, we use oneshot frequency estimation.

To design this system, we find the minimum phase error needed to satisfy the requirement ($\delta_{\sigma_e^2}$), then we find the shortest overhead to meet this phase error. Since, for fixed N , increasing σ_e^2 decreases the average BF gain and vice versa,

we determine $\delta_{\sigma_e^2}$ by applying the bisection method on (31). Then, using $\delta_{\sigma_e^2}$, we solve the problem $P2$ to determine the minimum overhead. If the minimum overhead makes the BF packet exceed the channel coherence time, the solution is not valid and we need to consider another alternative like increasing the transmit power. The minimum overheads obtained are shown in Fig. 8a for different distances. Then, we simulated the BF protocol at these SNRs using the waveforms obtained from $P2$ and plotted the empirical CDF of the destination SNR in Fig. 8b. We can see that the proposed solution approach (shown as solid lines) meets the required outage probability, which verifies the solution and all the underlying analysis. For a distance of 50 Km, we simulated the BF protocol using 0.8 the calculated minimum overheads (Ov) and 1.2 Ov, shown in Fig. 8b as dotted and dashed lines respectively. Shorter overheads violate the SNR requirements, and longer overheads exceeded them. This shows that using arbitrary waveform designs might either violate the requirements or use unnecessarily longer overheads.

IX. CONCLUSION

In this work, we developed and verified a mathematical framework to model the BF performance for a destination-led BF protocol. To derive this framework, we related the pre-BF SNR and preamble lengths to the combining phase error and then to the BF gain distribution. The proposed framework was verified experimentally using software-defined radios in a lab. Further, we demonstrated that BF from UAV-mounted-radios exceeded 80% of the ideal BF gains despite the short coherence time channel. Using the framework, for two example scenarios, we proposed approaches to design the number of BF radios and the length of the BF overheads and verified that they meet the requirements using simulations.

Even though we only considered a specific BF protocol and only two example scenarios, the proposed framework can support many protocol variations and use cases. For the protocol, the framework is applicable to any other choice of estimators as long as their phase error variance can be expressed mathematically. As for the scenarios, heuristics

can easily be developed to optimize over a combination of the SNR, preamble lengths, and the number of BF slaves, enabling the framework to adapt to many different deployment scenarios.

APPENDIX

A. Proof of Proposition 1

The variance error of the KF output is given by $p_{k|k}$ and we want to calculate its value. Substituting (17) into (21), we get $p_{k+1|k} = \frac{rp_{k|k-1}}{p_{k|k-1}+r} + q$. At steady state $p_{k+1|k} = p$ for all k and we get a simple form of the algebraic Riccati equation $p = \frac{rp}{p+r} + q$ [42]. Solving the equation, we get $p_{k+1|k} = p = \frac{q+r\sqrt{1+4\frac{r}{q}}}{2}$. Using (21), we get $\sigma_{fk}^2 = p_{k|k} = \frac{-q+q\sqrt{1+4\frac{r}{q}}}{2}$.

B. Proof of Proposition 2

$$G = \frac{1}{N} \left| \sum_{n=1}^N e^{j\phi_n^e} \right|^2 = \frac{1}{N} \sum_{n=1}^N e^{j\phi_n^e} \sum_{m=1}^N e^{-j\phi_m^e} \\ = 1 + \frac{2}{N} \sum_{m=1}^N \sum_{n=m+1}^N \cos(\phi_n^e - \phi_m^e) \quad (37)$$

Using the fact that for a zero mean Gaussian RV x , $\mathbb{E}\{\cos x\} = e^{-\text{var}\{x\}/2}$ [27], we get

$$\mathbb{E}\{G\} = 1 + (N-1)e^{-\sigma_e^2} \quad (38)$$

$$\text{var}\{G\} = \frac{4}{N^2} \text{var}\left\{ \sum_{m=1}^N \sum_{n=m+1}^N \cos(\phi_n^e - \phi_m^e) \right\} \\ = \frac{4}{N^2} \sum_{m=1}^N \sum_{n=m+1}^N \text{var}\{\cos(\phi_n^e - \phi_m^e)\} \\ + \frac{8}{N^2} \sum_{m=1}^N \sum_{n=m+1}^N \sum_{p=i+1}^N \text{cov}\{\cos(\phi_n^e - \phi_m^e), \cos(\phi_m^e - \phi_p^e)\} \quad (39)$$

$$= \frac{(N-1)}{N} (e^{-\sigma_e^2} - 1)^2 \left((e^{-\sigma_e^2} - 1)^2 + 2Ne^{-\sigma_e^2} \right) \quad (40)$$

where $\text{cov}\{x, y\}$ denotes the covariance of RVs x, y . Line (40) was obtained using the fact that $\text{var}\{\sum_{m=1}^M x_m\} = \sum_{m=1}^M \text{var}\{x_m\} + 2 \sum_{m=1}^M \sum_{n=m+1}^M \text{cov}\{x_m, x_n\}$ for any correlated M RVs x_m and by simplifying the summations. Line (41) uses the fact that for a zero mean Gaussian RV $\text{var}\{\cos x\} = \frac{1}{2}(e^{-\text{var}\{x\}} - 1)^2$ [27] and using that $\text{cov}\{\cos(\phi_n^e - \phi_m^e), \cos(\phi_m^e - \phi_p^e)\} = 0.5e^{-3\sigma_e^2} + 0.5e^{-\sigma_e^2} - e^{-2\sigma_e^2}$ as can be shown using the Gaussian RV relations from [27], the definition of covariance, and some trigonometric identities.

C. Proof of Proposition 3

We start by considering the simplified definition of G from (37). We rewrite the elements of the summation as the $N \times N$ matrix \mathbf{X} , such that its element $\mathbf{X}_{m,n} = \frac{2}{N} \cos(\phi_m - \phi_n)$. This yields $G = 1 + \sum_{m=1}^N \sum_{n=m+1}^N \mathbf{X}_{m,n}$. The summation is over the upper diagonal elements of the matrix.

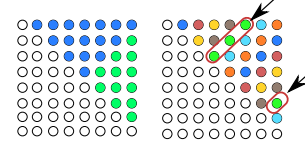


Fig. 9. Summation order for the matrix \mathbf{X} .

Our objective is to rewrite the inner sum as independent RVs of length proportional to N to invoke the central limit theory (CLT). To achieve that, we must avoid reusing the same value of ϕ_n^e in the inner sum, that is, the inner sum elements should have unique column and row indices.

$$\sum_{m=1}^N \sum_{n=m+1}^N \mathbf{X}_{m,n} = \sum_{n=2}^N \sum_{m=1}^{n-1} \mathbf{X}_{m,n} \quad (42)$$

$$= \sum_{n=2}^N \sum_{m=1}^{\min(n-1, N-n+1)} \mathbf{X}_{m,n} + \sum_{n=N/2+1}^N \sum_{m=N-n+1}^{n-1} \mathbf{X}_{m,n} \quad (43)$$

$$= \sum_{n=2}^N \left(\sum_{m=1}^{\lfloor n/2 \rfloor} \mathbf{X}_{m,n-m+1} + \sum_{m=1}^{\lfloor \frac{N+1-n}{2} \rfloor} \mathbf{X}_{N+1-(n-m+1), (N+1)-m} \right) \quad (44)$$

The summation in (42) rewrites the equation from column wise to row wise. In Line (43), we split the elements of the summation at the upward diagonal as illustrated in the first image of Fig. 9 for an 8×8 matrix. In Line (44), the inner summation is rewritten as two summations over the upward diagonal elements as shown in different colors in the second image of Fig. 9. From (44), each element of the inner summation consists of about $N/2$ terms² and none of the terms have common rows or columns, thus consist of independent RVs. We can rewrite the inner sum as the RV b_n as follows

$$b_n = \sum_{m=1}^{\lfloor n/2 \rfloor} \mathbf{X}_{m,n-m+1} + \sum_{m=1}^{\lfloor (N+1-n)/2 \rfloor} \mathbf{X}_{N+1-(n-m+1), (N+1)-m} \quad (45)$$

The variable b_n consists of identical independent RVs. Hence, for large N , the distribution of b_n converges to a Gaussian distribution. Lastly, we can rewrite G as $G = 1 + \sum_{n=2}^N b_n$. The variables b_n are correlated Gaussian RVs, hence their sum is Gaussian. This proves that for large N , G is Gaussian and its mean and variance are given by Proposition 2.

D. Proof of Proposition 4

We start this proof by considering the case of small σ_e^2 and then discuss the case of large N . Since ϕ_n are zero mean and assuming small σ_e^2 , $\phi_m - \phi_n$ is typically small and we can use the Taylor expansion of cosine around zero to simplify $\mathbf{X}_{m,n}$ (as defined in Appendix C) as $\mathbf{X}_{m,n} \approx \frac{2}{N} \left(1 - \frac{(\phi_m - \phi_n)^2}{2} \right)$. Then, we can rewrite (45) as $b_n = 2\frac{s_n}{N} - \chi_n$ where

²For odd N , the number of elements is either $N/2$ or $N/2 - 1$. This difference is insignificant for large N .

$s_n = \lfloor n/2 \rfloor + \lfloor (N+1-n)/2 \rfloor$ is the number of elements of b_n and $\chi_n = \frac{1}{N} \sum_{r=1}^{s_n} (\phi_{m_r} - \phi_{n_r})^2$ with m_r and n_r corresponding to the indexes from (45). The summation in χ_n is over independent zero mean Gaussian RVs that are squared, hence χ_n follows the Chi-squared distribution. We can rewrite G as

$$G = 1 + \frac{2}{N} \frac{N(N-1)}{2} - \sum_{n=2}^N \chi_n = N - X_\gamma \quad (46)$$

where $X_\gamma = \sum_{n=2}^N \chi_n$ is the sum of correlated Chi-squared RVs. The distribution of the summation of correlated Chi-squared RVs can be obtained using the Gamma distribution [43]. The shape K and scale θ parametrization of the resulting Gamma distribution can be calculated to realize the mean and variance of X_γ [44]. Using the mean and variance of G from Proposition 2, we get the following equations for the mean and variance respectively

$$K\theta = N - 1 - (N-1)e^{-\sigma_e^2} \quad (47)$$

$$K\theta^2 = \frac{(N-1)}{N} (1 - e^{-\sigma_e^2})^2 \left((1 - e^{-\sigma_e^2})^2 + 2Ne^{-\sigma_e^2} \right) \quad (48)$$

Solving these two equations, we get the values of K and θ in (29) and (30). This proof is based on the assumption that σ_e^2 is small. For large values of N , K becomes large, and the Gamma distribution converges to a Gaussian distribution with mean $K\theta$ and variance $K\theta^2$ [45], which is the true distribution of G as shown in Proposition 3.

REFERENCES

- [1] R. Mudumbai, G. Barriac, and U. Madhow, "On the feasibility of distributed beamforming in wireless networks," *IEEE Trans. Wireless Commun.*, vol. 6, no. 5, pp. 1754–1763, May 2007.
- [2] R. Mudumbai, D. R. B. Iii, U. Madhow, and H. V. Poor, "Distributed transmit beamforming: Challenges and recent progress," *IEEE Commun. Mag.*, vol. 47, no. 2, pp. 102–110, Feb. 2009.
- [3] S. Jayaprakasam, S. K. A. Rahim, and C. Y. Leow, "Distributed and collaborative beamforming in wireless sensor networks: Classifications, trends, and research directions," *IEEE Commun. Surveys Tuts.*, vol. 19, no. 4, pp. 2092–2116, 4th Quart., 2017.
- [4] G. Skorobogatov, C. Barrado, and E. Salami, "Multiple UAV systems: A survey," *Unmanned Syst.*, vol. 8, no. 2, pp. 149–169, Apr. 2020.
- [5] A. Muralidharan and Y. Mostofi, "Energy optimal distributed beamforming using unmanned vehicles," *IEEE Trans. Control Netw. Syst.*, vol. 5, no. 4, pp. 1529–1540, Dec. 2018.
- [6] L. Bertizzolo, E. Demirors, Z. Guan, and T. Melodia, "CoBeam: Beamforming-based spectrum sharing with zero cross-technology signaling for 5G wireless networks," in *Proc. IEEE Conf. Comput. Commun. (INFOCOM)*, Jul. 2020, pp. 1429–1438.
- [7] Y.-S. Tu and G. J. Pottie, "Coherent cooperative transmission from multiple adjacent antennas to a distant stationary antenna through AWGN channels," in *Proc. IEEE 55th Vehicular Technol. Conf. (VTC Spring)*, vol. 1, May 2002, pp. 130–134.
- [8] R. Mudumbai, J. Hespanha, U. Madhow, and G. Barriac, "Distributed transmit beamforming using feedback control," *IEEE Trans. Inf. Theory*, vol. 56, no. 1, pp. 411–426, Jan. 2010.
- [9] D. R. Brown, III, and H. V. Poor, "Time-slotted round-trip carrier synchronization for distributed beamforming," *IEEE Trans. Signal Process.*, vol. 56, no. 11, pp. 5630–5643, Nov. 2008.
- [10] S. Leak *et al.*, "Distributed transmit beamforming expanding the capacity and range of tactical communications," in *Proc. Mil. Commun. Inf. Syst. Conf. (MilCIS)*, Nov. 2018, pp. 1–6.
- [11] D. Kramarev *et al.*, "Event-triggered synchronization for mobile distributed transmit beamforming," in *Proc. IEEE Mil. Commun. Conf. (MILCOM)*, Nov. 2019, pp. 343–348.
- [12] M. M. Rahman, H. E. Baidoo-Williams, R. Mudumbai, and S. Dasgupta, "Fully wireless implementation of distributed beamforming on a software-defined radio platform," in *Proc. ACM/IEEE 11th Int. Conf. Inf. Process. Sensor Netw. (IPSN)*, Apr. 2012, pp. 305–316.
- [13] F. Quitin, U. Madhow, M. M. U. Rahman, and R. Mudumbai, "Demonstrating distributed transmit beamforming with software-defined radios," in *Proc. IEEE Int. Symp. World Wireless, Mobile Multimedia Netw. (WoWMoM)*, Jun. 2012, pp. 1–3.
- [14] S. Mohanti, E. Bozkaya, M. Y. Naderi, B. Canberk, G. Secinti, and K. R. Chowdhury, "WiFED mobile: WiFi friendly energy delivery with mobile distributed beamforming," *IEEE/ACM Trans. Netw.*, vol. 29, no. 3, pp. 1362–1375, Jun. 2021.
- [15] Y. Khosiawan and I. Nielsen, "A system of UAV application in indoor environment," *Prod. Manuf. Res.*, vol. 4, no. 1, pp. 2–22, Jan. 2016.
- [16] H. Yan, S. Hanna, K. Balke, R. Gupta, and D. Cabric, "Software defined radio implementation of carrier and timing synchronization for distributed arrays," in *Proc. IEEE Aerosp. Conf.*, Mar. 2019, pp. 1–12.
- [17] S. Mohanti *et al.*, "AirBeam: Experimental demonstration of distributed beamforming by a swarm of UAVs," in *Proc. IEEE MASS*, Nov. 2019, pp. 162–170.
- [18] S. R. Mghabghab and J. A. Nanzer, "Impact of VCO and PLL phase noise on distributed beamforming arrays with periodic synchronization," *IEEE Access*, vol. 9, pp. 56578–56588, 2021.
- [19] F. Quitin, M. M. U. Rahman, R. Mudumbai, and U. Madhow, "A scalable architecture for distributed transmit beamforming with commodity radios: Design and proof of concept," *IEEE Trans. Wireless Commun.*, vol. 12, no. 3, pp. 1418–1428, Mar. 2013.
- [20] J. Kong, F. T. Dagefu, and B. M. Sadler, "Simultaneous beamforming and nullforming for covert wireless communications," in *Proc. IEEE 91st Vehicular Technol. Conf. (VTC-Spring)*, May 2020, pp. 1–6.
- [21] S. M. Ellison, S. R. Mghabghab, and J. A. Nanzer, "Multi-node open-loop distributed beamforming based on scalable, high-accuracy ranging," *IEEE Sensors J.*, vol. 22, no. 2, pp. 1629–1637, Jan. 2021.
- [22] H. Ochiai, P. Mitran, H. V. Poor, and V. Tarokh, "Collaborative beamforming for distributed wireless ad hoc sensor networks," *IEEE Trans. Signal Process.*, vol. 53, no. 11, pp. 4110–4124, Nov. 2005.
- [23] T. Feng, L. Xie, J. Yao, and J. Xu, "UAV-enabled data collection for wireless sensor networks with distributed beamforming," *IEEE Trans. Wireless Commun.*, vol. 21, no. 2, pp. 1347–1361, Feb. 2022.
- [24] G. Sklivanitis, K. Alexandris, and A. Bletsas, "Testbed for non-coherent zero-feedback distributed beamforming," in *Proc. IEEE Int. Conf. Acoust., Speech Signal Process.*, May 2013, pp. 2563–2567.
- [25] J. George, A. Parayil, C. T. Yilmaz, B. L. Allik, H. Bai, and A. Chakraborty, "Multi-agent coordination for distributed transmit beamforming," in *Proc. Amer. Control Conf.*, Jul. 2020, pp. 144–149.
- [26] S. Hanna, E. Krijestorac, and D. Cabric, "Destination-feedback free distributed transmit beamforming using guided directionality," *IEEE Trans. Mobile Comput.*, early access, Jul. 5, 2022, doi: 10.1109/TMC.2022.3188602.
- [27] D. R. Brown, P. Bidigare, and U. Madhow, "Receiver-coordinated distributed transmit beamforming with kinematic tracking," in *Proc. IEEE Int. Conf. Acoust., Speech Signal Process. (ICASSP)*, Mar. 2012, pp. 5209–5212.
- [28] J. Elson, L. Girod, and D. Estrin, "Fine-grained network time synchronization using reference broadcasts," *ACM SIGOPS Operating Syst. Rev.*, vol. 36, pp. 147–163, Dec. 2003.
- [29] B. Williams and T. Camp, "Comparison of broadcasting techniques for mobile ad hoc networks," in *Proc. 3rd ACM Int. Symp. Mobile ad hoc Netw. Comput. (MobiHoc)*, New York, NY, USA, 2002, pp. 194–205.
- [30] G. W. Lank, I. S. Reed, and G. E. Pollon, "A semicoherent detection and Doppler estimation statistic," *IEEE Trans. Aerosp. Electron. Syst.*, vol. AES-9, no. 2, pp. 151–165, Mar. 1973.
- [31] N. A. Thacker and A. Lacey, "Tutorial: The Kalman filter," *Imag. Sci. Biomed. Eng. Division, Med. School, Citeseer, Univ. Manchester, Manchester, U.K.*, 1998, p. 61.
- [32] S. Tretter, "Estimating the frequency of a noisy sinusoid by linear regression (corresp.)," *IEEE Trans. Inf. Theory*, vol. IT-31, no. 6, pp. 832–835, Nov. 1985.
- [33] D. W. Matolak and R. Sun, "Air-ground channel characterization for unmanned aircraft systems—Part III: The suburban and near-urban environments," *IEEE Trans. Veh. Technol.*, vol. 66, no. 8, pp. 6607–6618, Aug. 2017.

- [34] L. Cao and H. M. Schwartz, "Exponential convergence of the Kalman filter based parameter estimation algorithm," *Int. J. Adapt. Control Signal Process.*, vol. 17, no. 10, pp. 763–783, 2003.
- [35] GNU Radio Website. *GNU Radio*. Accessed: Sep. 2021. [Online]. Available: <https://gnuradio.org/>
- [36] V. Va and R. W. Heath, Jr., "Basic relationship between channel coherence time and beamwidth in vehicular channels," in *Proc. IEEE VTC*, Sep. 2015, pp. 1–5.
- [37] S. Boyd and L. Vandenberghe, *Convex Optimization*. Cambridge, U.K.: Cambridge Univ. Press, 2004.
- [38] M. Grant and S. Boyd. (Mar. 2014). *CVX: MATLAB Software for Disciplined Convex Programming, Version 2.1*. [Online]. Available: <http://cvxr.com/cvx>
- [39] A. Trotta, U. Muncuk, M. Di Felice, and K. R. Chowdhury, "Persistent crowd tracking using unmanned Aerial vehicle swarms: A novel framework for energy and mobility management," *IEEE Veh. Technol. Mag.*, vol. 15, no. 2, pp. 96–103, Jun. 2020.
- [40] A. Goldsmith, *Wireless Communications*. Cambridge, U.K.: Cambridge Univ. Press, 2005.
- [41] Y. Chakkour, H. Fernández, V. M. R. Peñarocha, L. Rubio, and J. Reig, "Coherence time and Doppler spread analysis of the V2V channel in highway and urban environments," in *Proc. IEEE Int. Symp. Antennas Propag. USNC/URSI Nat. Radio Sci. Meeting*, Jul. 2018, pp. 373–374.
- [42] D. P. Bertsekas, *Dynamic Programming and Optimal Control*, vol. 1. Belmont, MA, USA: Athena Scientific, 2000.
- [43] N. H. Gordon and P. F. Ramig, "Cumulative distribution function of the sum of correlated chi—Squared random variables," *J. Stat. Comput. Simul.*, vol. 17, no. 1, pp. 1–9, Jan. 1983.
- [44] A. Ferrari, "A note on sum and difference of correlated chi-squared variables," 2019, *arXiv:1906.09982*.
- [45] A. DasGupta, *Normal Approximations and the Central Limit Theorem*. New York, NY, USA: Springer, 2010, pp. 213–242.



Samer Hanna (Member, IEEE) received the B.Sc. degree in electrical engineering and the M.Sc. degree in engineering mathematics from Alexandria University, Alexandria, Egypt, in 2013 and 2017, respectively, and the Ph.D. degree from the University of California, Los Angeles, CA, USA, in 2021. His research interests include the applications of machine learning in wireless communications and coordinated communications using unmanned aerial vehicles.



Danijela Cabric (Fellow, IEEE) received the M.S. degree in electrical engineering from the University of California, Los Angeles (UCLA), in 2001, and the Ph.D. degree in electrical engineering from UC Berkeley in 2007. She is a Professor in electrical and computer engineering with UCLA. Her research interests include millimeter-wave communications, distributed communications and sensing for the Internet of Things, and machine learning for wireless networks co-existence and security. She received the Samuelli Fellowship in 2008, the Okawa Foundation Research Grant in 2009, the Hellman Fellowship in 2012, the National Science Foundation Faculty Early Career Development (CAREER) Award in 2012, and the Qualcomm Faculty Award in 2020 and 2021. She was an Associate Editor of IEEE TRANSACTIONS ON COGNITIVE COMMUNICATIONS AND NETWORKING, IEEE TRANSACTIONS ON WIRELESS COMMUNICATIONS, IEEE TRANSACTIONS ON MOBILE COMPUTING, IEEE *Signal Processing Magazine*, and IEEE ComSoc Distinguished Lecturer.